

Research Paper

Microbial sulfate reduction regulated by relative sea level change in a Pleistocene – Holocene sedimentary record: Insights from Loch Duart, Scotland, UK

L.G. Podrecca^{a,*}, A.L. Masterson^a, M.T. Hurtgen^a, J. Taylor^b, J.M. Lloyd^c, D. Selby^b, B.B. Sageman^a

^a Northwestern University, Department of Earth & Planetary Sciences, Evanston, IL, USA

^b Durham University, Department of Earth Sciences, Durham DH1 3LE, UK

^c Durham University, Department of Geography, Durham DH1 3LE, UK

ARTICLE INFO

Editor: Dr. Hailiang Dong

Keywords:

Sulfur isotope geochemistry
Osmium isotope geochemistry
Geochemical proxies tracking degree of marine connectivity and local redox conditions
Novel S-isotope relationships (metal sulfides and organic sulfur)
Paleoclimatology
Holocene deglaciation
Eustasy and relative sea level change

ABSTRACT

A Pleistocene–Holocene-aged sediment core recovered near Loch Duart, located in the coastal Assynt region of NW Scotland, UK, provides new insight into the relationship between the sulfur isotope composition of iron sulfides (pyrite) and organic sulfur under rapidly changing environmental conditions. Since the Late Glacial period, shifts in local marine connectivity at Loch Duart have been driven by the competition between two fundamental Earth surface processes: eustatic sea level rise due to post-glacial meltwater contributions since the Last Glacial Maximum and relative sea level (RSL) fall associated with glacial isostatic rebound. These processes, imprinted on the sedimentary record, have been evaluated via lithology, microfossil assemblages, elemental analysis, and isotopic measurements. Over the last 17 kyr, Loch Duart has transitioned from (1) marine conditions, when eustatic rise due to deglaciation exceeded glacial isostatic rebound, to (2) non-marine conditions, where land uplift caused by isostatic rebound exceeded eustatic rise, to (3) marine conditions, as the eustatic contribution outpaced isostatic rebound, followed by (4) brackish-water conditions, as the eustatic contribution reduced while glacial isostatic uplift continued, with marine inundation limited to part of the tidal cycle at the present day.

Here, we evaluate marked perturbations in the local sulfur (S) cycle related to the aforementioned environmental changes. The marine interval coincides with relatively stable and low $\delta^{34}\text{S}_{\text{sulfide}}$ values (average ~ -27.2 ‰), the non-marine interval records an abrupt positive $\delta^{34}\text{S}_{\text{sulfide}}$ excursion of over 30 ‰ (average ~ 9 ‰), and the brackish interval preserves intermediate values (average ~ -16.2 ‰). The $\delta^{34}\text{S}_{\text{org}}$ values shift sympathetically with $\delta^{34}\text{S}_{\text{sulfide}}$, although the magnitude of $\delta^{34}\text{S}_{\text{org}}$ change is nominal by comparison, particularly during the transition from freshwater to marine facies. As expected, marine and brackish sections preserve higher $\delta^{34}\text{S}_{\text{org}}$ values than coeval $\delta^{34}\text{S}_{\text{sulfide}}$. Interestingly, this relationship is reversed in the freshwater facies, where sulfides are ^{34}S -enriched relative to organic S by as much as 20 ‰, suggesting that RSL modulates the isotopic composition of non-pyrite phases in the bulk S pool. We hypothesize that this inverse relationship ($\delta^{34}\text{S}_{\text{org}} < \delta^{34}\text{S}_{\text{sulfide}}$) may arise from a spatial decoupling of pyrite and organic S formation within the water column and/or sediments in a system with low sulfate concentrations. Evaluating shifts in the local S-cycle associated with RSL changes allows for a novel comparison between S and osmium isotope records, demonstrating that these proxies may have joint applications for paleoenvironmental investigations in shallow coastal systems. We offer new perspectives on the interplay between eustasy, RSL, and the S-cycle by assessing these relationships in a coastal isolation basin.

* Corresponding author.

E-mail address: lucapodrecca2024@u.northwestern.edu (L.G. Podrecca).

<https://doi.org/10.1016/j.chemgeo.2025.122633>

Received 6 September 2024; Received in revised form 16 January 2025; Accepted 18 January 2025

Available online 21 January 2025

0009-2541/© 2025 The Authors. Published by Elsevier B.V. This is an open access article under the CC BY license (<http://creativecommons.org/licenses/by/4.0/>).

1. Introduction

The biogeochemical sulfur (S) cycle is intimately linked to several of the most important processes in Earth's history. The S isotope ($\delta^{34}\text{S}$) record of various S phases (i.e., barite, carbonate-associated sulfate, gypsum/anhydrite, and sedimentary pyrite) has been utilized to investigate the origins of life (Shen et al., 2001; Philipot et al., 2007), the accumulation of oxygen in the ocean and atmosphere (Berner and Raiswell, 1983; Holser et al., 1989; Canfield and Teske, 1996; Canfield, 1998, 2001; Canfield and Raiswell, 1999), and changes in the redox state of Earth's surface. This biogeochemical cycle is regulated by several metabolic processes, including microbial sulfate reduction (MSR), sulfide oxidation, and the disproportionation of intermediate S species (Bak and Cypionka, 1987; Canfield and Teske, 1996; Tsang et al., 2023). Consequently, environmental controls that geochemically

influence these metabolisms are imprinted on the aforementioned geological archives. It is through these pathways, mainly via the remineralization of organic matter during MSR, that the S cycle engages with the global carbon (C) and oxygen (O) cycles.

Organic Matter (OM) burial is a key driver controlling Earth's surface oxygen budget (Holland, 1973). Thus, mechanisms impacting the rates of primary production and the efficiency of OM preservation play an important role in regulating the concentration of atmospheric O_2 and CO_2 . The primary production of OM in surface waters is largely a function of the availability of limiting nutrients (Fe, N, P). The efficiency of transporting this OM to bottom waters is strongly influenced by the duration of O_2 exposure, with longer exposure times increasing the period over which OM is susceptible to remineralization by aerobic heterotrophs (Hartnett et al., 1998). The burial efficiency of OM is enhanced through adsorption to mineral surfaces (Hemingway et al.,



Fig. 1. Map of the region with field site location indicated by yellow star (from Taylor et al., 2024). (For interpretation of the references to colour in this figure legend, the reader is referred to the web version of this article.)

2019) or through chemical alteration into larger, less-functionalized molecules (Hartnett et al., 1998). The later process, termed organic matter sulfurization, may have influenced organic carbon preservation during different periods in Earth's history (Raven et al., 2018, Raven et al., 2019, 2021, 2023). Key to understanding the competitive balance between the biogeochemical processes controlling the S cycle are local records that reflect the balance between OM burial, MSR, and S loss pathways, including pyrite formation and OM sulfurization.

1.1. Geologic background and setting

Loch Duart (NW Scotland, UK; Fig. 1) is an isolation basin, defined as a topographic depression characterized by intermittent sea connectivity due to RSL changes (Long et al., 2011). Over the last 17 kyrs, environmental change in the region has been driven by the collapse and deglaciation of the British and Irish Ice Sheet (BIIS). This deglaciation has fostered two competing processes: global meltwater-fed eustatic sea level rise and isostatic-rebound-driven RSL fall. The combination of these two processes controls variations in relative sea level change at Loch Duart, producing the lithofacies succession of marine (Lithofacies 1; L1) to freshwater (Lithofacies 2; L2), and back to marine (Lithofacies 3; L3) before transitioning into a modern brackish-tidal setting (Lithofacies 4; L4) (Taylor et al., 2024). Each unit, defined by microfossil assemblages (Hamilton et al., 2015; Taylor et al., 2024), preserves a distinct geochemical fingerprint reflecting the degree of connectivity with the open ocean. The sedimentary record is anchored by exceptional biostratigraphic histories (Hamilton et al., 2015; Taylor et al., 2024) and a newly constructed radiocarbon chronology (Taylor et al., 2024). The latter underpins an investigation of the relationship between RSL and changes in local water column/bottom water chemistry through a well-constrained geochronologic window that we expand upon to test the controls on the S cycle.

1.2. Microbial Sulfate Reduction (MSR)

MSR is an anaerobic process where microbes remineralize organic matter (OM, expressed below as CH_2O) and reduce sulfate (SO_4^{2-}) to sulfide (H_2S).



Through the Phanerozoic, this process regulates atmospheric O_2 concentrations (Berner, 1989), providing a critical interface between the exogenic C, O, and S cycles. Rates of sediment-hosted MSR are enhanced by increased delivery of OM to bottom waters and consequent O_2 depletion. Increased OM-flux through the water column can induce anoxic bottom water conditions by driving oxygen consumption by aerobic decomposers. Once available oxygen is depleted, OM decomposition continues via MSR. Thus, increased OM delivery to sediments is associated with increased dissolved sulfide production, which can either be re-oxidized to intermediate S species (elemental S, polysulfides, thiosulfate) and/or sulfate (Friedrich et al., 2001, 2005), react with organic material to form organic S compounds via sulfurization (Sinninghe Damste and De Leeuw, 1990), or be scavenged by reactive metals, such as (Fe), to form sedimentary sulfides (e.g., Berner, 1989; Seal, 2006; Fike et al., 2015). These reduced S-species and their associated metabolisms can, in turn, enhance OM preservation by limiting aerobic remineralization (Berner and Raiswell, 1983). Additionally, it has been proposed that the "sulfurization" of labile organic molecules into more recalcitrant forms may further enhance OM preservation (Sinninghe Damste and De Leeuw, 1990; Hartgers et al., 1997). These connections link perturbations in the surface S-cycle to those in the C cycle, the porewater oxygen budget, and the redox state near the sediment-water interface (SWI).

A kinetic isotope effect (KIE) accompanies MSR, as obligate anaerobes preferentially dissimilate ^{32}S (over ^{34}S) during dissolved sulfide

production. This biologically mediated isotope fractionation can cause dissolved sulfides to become ^{34}S -depleted relative to sulfate by as much as ~ 70 ‰ (Goldhaber and Kaplan, 1980; Wortmann et al., 2001; Brunner and Bernasconi, 2005; Sim et al., 2011a). The resulting dissolved sulfide may then react with iron to form ^{34}S -depleted pyrite (FeS_2). The magnitude of the KIE associated with MSR (ϵ_{msr}) is influenced by two primary mechanisms: the concentration of sulfate in the local environment (Habicht et al., 2002) and the cell-specific sulfate reduction rate (e.g., Leavitt et al., 2013; Wing and Halevy, 2014; Bradley et al., 2016), which reflects the relative sulfate flux into, and back out of, the cell (Brunner and Bernasconi, 2005). When MSR occurs in environments where sulfate is low ($< 200 \mu\text{M}$), ϵ_{msr} may be significantly diminished, and the S isotopic composition of the dissolved sulfide approaches that of sulfate (Habicht et al., 2002; Crowe et al., 2014). Greater cell-specific sulfate reduction rates, facilitated by increased availability and/or lability of organic matter, reduce the sulfate flux into the cell relative to the flux out of the cell, which ultimately lowers ϵ_{msr} (Harrison and Thode, 1958; Kaplan and Rittenberg, 1964; Brunner and Bernasconi, 2005; Sim et al., 2011a, 2011b; Leavitt et al., 2013).

In evaluating S isotope records of sulfate and sulfide, it is essential to distinguish between ϵ_{msr} and what is referred to as the reservoir effect (e.g., Gomes and Hurtgen, 2013). The production of dissolved sulfide via MSR occurs across different depths of euxinic water columns (syngenetic) and/or sediments (diagenetic). As sulfate is consumed during MSR, sulfate concentrations decrease, and the S isotope composition of the residual sulfate pool increases as microbes preferentially remove ^{32}S during the production of dissolved sulfide (i.e., Rayleigh fractionation; Fig. 2). As the fraction of sulfate remaining in the system (f) decreases, the S isotope composition of subsequently produced dissolved sulfide must increase (assuming ϵ_{msr} remains constant). Importantly, sulfate levels play a critical role in determining the rate at which the S isotope composition of sulfate and dissolved sulfide evolves to higher $\delta^{34}\text{S}$ values with increasing depth in the water column/sediments. In high sulfate systems, f decreases less rapidly with depth and the S isotope

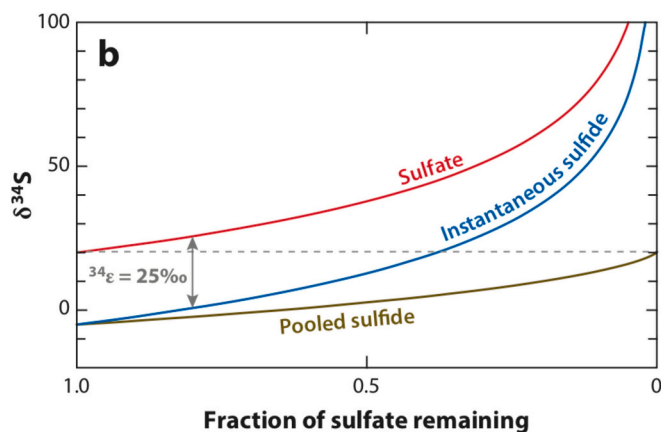


Fig. 2. Rayleigh plot of the S isotopic evolution of sulfate and sulfide versus the fraction of sulfate remaining resulting from MSR (with constant ϵ_{msr}). The blue line represents the S isotope composition of the instantaneously generated dissolved sulfide, whereas the grey line tracks the S isotope composition of the pooled (average) sulfide. As sulfate is consumed during MSR in a local reservoir (e.g., sediment pore spaces or water column of an anoxic basin) and the fraction of sulfate remaining (f) decreases, the S isotope composition of the residual sulfate pool becomes progressively higher. As f in the local reservoir decreases, the S isotope value of subsequently produced sulfide must increase (assuming the magnitude of S isotope fraction associated with MSR remains constant). As f approaches zero, the total pooled $\delta^{34}\text{S}_{\text{sulfide}}$ value approaches the S isotope value of the original sulfate pool (Ohmoto and Goldhaber, 1997; Canfield, 2001). (Figure modified from Fike et al., 2015.) (For interpretation of the references to colour in this figure legend, the reader is referred to the web version of this article.)

composition of MSR-generated sulfide evolves to higher values more slowly (Fig. 3a). By contrast, in low sulfate systems (while holding other variables constant), f decreases rapidly with depth and thus the rate of $\delta^{34}\text{S}_{\text{sulfide}}$ increase is also more rapid (Fig. 3b). Therefore, even in a system where the KIE associated with MSR and all other variables remain constant, the reservoir effect can strongly influence the preserved $\delta^{34}\text{S}_{\text{sulfide}}$ values (Halevy et al., 2023).

The system's "degree of openness" to sulfate replenishment significantly influences the reservoir effect. For instance, sulfate can be replenished more readily in the water column (as opposed to sediment pore spaces) due to active circulation within the water column; this "openness" thus reduces the significance of the reservoir effect and promotes the formation of ^{34}S -depleted dissolved sulfide (relative to diagenetic sulfide production). By contrast, the "degree of openness" is much lower in sediment pore spaces, as diffusion rates hinder sulfate replenishment. Thus, MSR occurring in sediment pore spaces, and especially pore spaces being rapidly buried by high sedimentation rates, experience an amplified reservoir effect, which promotes the production of ^{34}S -enriched dissolved sulfide (relative to syngenetic sulfide production) (Goldhaber and Kaplan, 1975; Maynard, 1980; Gautier, 1986; Claypool, 2004).

1.3. Organic Sulfur (S_{org})

Assimilatory sulfate reduction plays a key role in creating amino acids (cysteine and methionine) and is thus associated with all known life (Roy and Trudinger, 1970). Organic matter sulfurization, however, refers to reactions between inorganic S species (dissolved sulfides and intermediate S species) and organic matter, whereby certain reactive functional groups, common in lipids and carbohydrates, are replaced with S-species (Sinninghe Damste and De Leeuw, 1990). Sulfurization of OM can occur in anoxic and sulfidic (euxinic) settings; the process decreases the reactivity of OM by increasing the size of the polymeric compounds relative to the preexisting organic molecules (Sinninghe Damsté and de Leeuw, 1990), effectively increasing the preservation potential of organic molecules (Werne et al., 2004; Hülse et al., 2019).

Organic S (S_{org}) is one of the most abundant reduced S-species in the sedimentary record, second only to pyrite (Anderson and Pratt, 1995). Like pyrite, the S isotope composition of S_{org} ($\delta^{34}\text{S}_{\text{org}}$) is regulated by the

S isotope composition of the "parent" S-phase, in this case, dissolved sulfide produced via MSR and associated reactive intermediate S species (Werne et al., 2008). However, while minimal isotopic fractionation occurs during iron sulfidation (Wilkin and Barnes, 1996), $\delta^{34}\text{S}_{\text{org}}$ values tend to be ^{34}S -enriched relative to dissolved sulfide (Amrani et al., 2008). This enrichment is estimated to average $\sim 10\text{‰}$ (Anderson and Pratt, 1995), although enrichments of up to 38 ‰ have been preserved in the sedimentary record (Shawar et al., 2018). S_{org} can form either syngenetically in the water column ("open system") or diagenetically within the anoxic portions of sediments ("closed system") and the S isotope composition of S_{org} will depend on where in the water column and/or sediments it formed (e.g. Raven et al., 2019). For example, diagenetic S_{org} production is generally associated with increasing S_{org} concentration and $\delta^{34}\text{S}_{\text{org}}$ values with depth in the sediments (Werne et al., 2000; Raven et al., 2015), similar to the $\delta^{34}\text{S}$ versus depth relationship for MSR-generated dissolved sulfide and pyrite (Fig. 3a). In rare instances, lower $\delta^{34}\text{S}_{\text{org}}$ values relative to coeval pyrite have been recorded (Brüchert and Pratt, 1996; Raven et al., 2015; Raven et al., 2023).

In Fig. 3, we present a schematic illustration of the reservoir effect and the relationships among ϵ_{msr} and the S isotope composition of sulfate, sulfide, and S_{org} with depth under variable environmental conditions (sulfate concentration and water column redox). This topic, including potential mechanisms for generating $\delta^{34}\text{S}_{\text{org}}$ values that are lower than co-existing $\delta^{34}\text{S}_{\text{sulfide}}$ values, will be discussed in greater detail below.

1.4. Osmium

Osmium has a short oceanic residence time (1000–10,000 years; Peucker-Ehrenbrink and Ravizza, 2000; Rooney et al., 2016) and two easily distinguished isotopic end-member reservoirs: the mantle and the continental crust. These characteristics make it an attractive proxy for assessing paleoceanographic change (Peucker-Ehrenbrink and Ravizza, 2000). The mantle possesses an unradiogenic $^{187}\text{Os}/^{188}\text{Os}$ composition (~ 0.12), whereas crustal sources are characterized by more radiogenic values (≥ 1.4 ; Peucker-Ehrenbrink and Ravizza, 2000). The relative contribution of these distinct sources to the marine realm produces an average $^{187}\text{Os}/^{188}\text{Os}$ value of 1.04–1.06 for modern open seawater

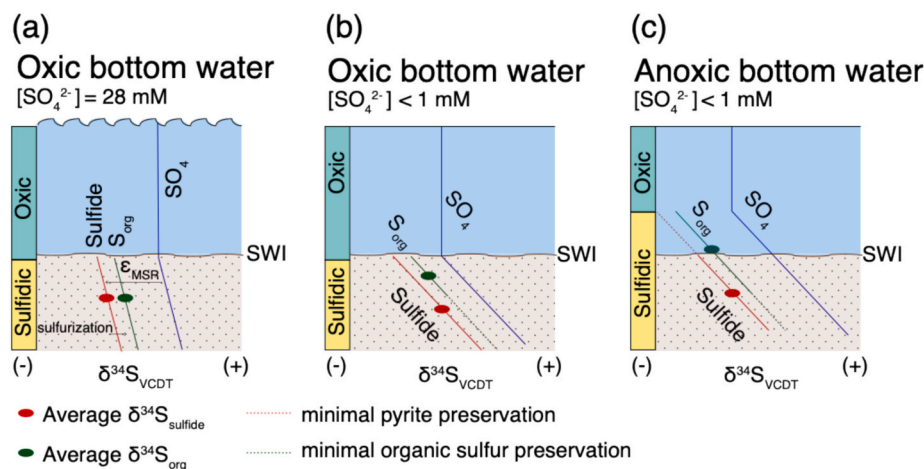


Fig. 3. Schematic illustration of the reservoir effect under different environmental conditions: (a) under oxidic water column conditions with high sulfate concentrations. " ϵ_{msr} " represents the KIE associated with MSR, while "sulfurization" refers to isotope fractionation during organic matter sulfurization. (b) Isolation from the marine reservoir (as in L2) prevents sulfate replenishment, forcing ongoing MSR to increasingly utilize ^{34}S -enriched sulfate. This is illustrated by the relatively steep slopes of the three S-phases (sulfide, S_{org} , and sulfate). The relative positioning of the average $\delta^{34}\text{S}_{\text{org}}$ and $\delta^{34}\text{S}_{\text{sulfide}}$ values reflects the temporal offset, where the organic fraction captures earlier more ^{34}S -depleted dissolved sulfide, while the sulfide (pyrite) fraction reflects the dominance of a later ^{34}S -enriched diagenetic component. (c) This scenario is similarly characterized by low sulfate conditions. Unlike (b), this scenario has anoxic bottom waters as well. Again, S_{org} captures the earliest (most ^{34}S -depleted) dissolved sulfide produced during MSR (in the water column), while the sulfide (pyrite) record reflects ^{34}S -enriched dissolved sulfide generated in the sediment pore spaces. Thus, both scenarios (b) and (c) invoke the same mechanism to explain the relationship between $\delta^{34}\text{S}_{\text{org}}$ and $\delta^{34}\text{S}_{\text{sulfide}}$ (low sulfate concentration) under different environmental conditions.

(Sharma et al., 1997; Peucker-Ehrenbrink and Ravizza, 2000; Rooney et al., 2016 and references therein). Alongside our sulfur study, we utilize an osmium isotope ($^{187}\text{Os}/^{188}\text{Os}$) record from a previous study of Loch Duart (Taylor et al., 2024, which underpins the state of local marine connectivity at the depositional site from the Late Pleistocene through the Holocene.

2. Material and methods

In 2020, a 220 cm sediment core (Loch Duart Marsh 20-JT – hereafter LDM 20-JT; see Taylor et al., 2024) was recovered from the present-day salt marsh at Loch Duart. The core was obtained using a side-filling, chambered-type “Russian” core sampler and the recovered sediments spanning the Late Glacial period to the present day, providing an opportunity to evaluate paleoenvironmental changes associated with the deglaciation of the BHS. Notably, LDM 20-JT was recovered 3 m southeast of a previous Russian core location (LDM 13-1) that produced a robust diatom-based biostratigraphic study (Hamilton et al., 2015). Together, these studies provide the paleoenvironmental framework that underpins our interpretations of the sulfur cycle.

2.1. Geochemical analyses

Bulk sediment samples from the LDM-20-JT core were oven-dried (50 °C), and then crushed and homogenized using an agate pestle and mortar. For this study, sample powders underwent weight percent analysis for S_{sulfide} and S_{org} , as well as stable isotope measurements of $\delta^{34}S_{\text{sulfide}}$ and $\delta^{34}S_{\text{org}}$. A previous study analyzed the powders for wt% TOC and $\delta^{13}C_{\text{org}}$ (Taylor et al., 2024), which, in addition to the osmium isotope data, are presented here alongside the S data (Fig. 4).

Chromium reducible S (Zhabina and Volkov, 1978; Canfield et al., 1986; Gröger et al., 2009) is the standard protocol for the extraction and reductive distillation of S and sulfides from sediments via hot chromium chloride, which converts sedimentary S-phases (e.g., elemental S, FeS and FeS₂) to Ag₂S for $\delta^{34}S$ analysis. This process combines the various reducible S phases into a single pool, complicating interpretations of S isotope results. Elemental sulfur (S_{el}) is largely insoluble in water and in most organic solvents, except for a S-containing solvent (CS₂). Our

protocol is designed to quantitatively extract S_{el} from sediment samples, allowing for isotopic analysis of S_{el} and further extraction of S-phases previously extracted for S_{el} .

Samples were weighed (~ 1.0 g) into Exetainer vials and subsequently filled with a 50/50 mix of CS₂ and acetone. The supernatant was then transferred into a silica wool-packed pipette and drained into a round-bottom flask containing ~1.0 g of diatomaceous earth; this step was repeated until the diatomaceous earth became visibly saturated with solvent (~3 mL/g). Samples were left in a fume hood for 24 h to ensure complete evaporation of the solvent before proceeding with the CRS procedure. The original sample material remaining in the Exetainer vials, now “desulfurized”, underwent additional rounds of chemistry to extract AVS (via the CRS method described below, without the step utilizing chromium (II) chloride) and sulfide phases without the S_{el} component. However, neither the AVS nor the S_{el} phases were extracted in quantities that could confidently be distinguished from blanks during Cline analysis (Cline, 1969) or that would allow for isotopic measurements; thus, they are not discussed further.

This chromium reducible S (CRS) procedure recovers various pools of reduced inorganic S (e.g., pyrite) present in crushed sediments, including elemental sulfur and iron monosulfide phases, by reacting the sample material in 20 mL of 1 M chromium (II) chloride (CrCl₂) solution, which is acidified to 0.5 N hydrochloric acid (HCl) for 2 h under a nitrogen atmosphere. The process liberates the trapped S species as hydrogen sulfide (H₂S), which travels through a specialized glass line to be captured in a trapping flask containing a 0.3 M zinc (Zn) acetate solution, thereby forming a relatively stable zinc sulfide (ZnS) product. An aliquot of this ZnS product-solution (4 mL) is partitioned for well-plate analysis, described below, with the remaining ZnS subjected to 1 mL of silver nitrate (AgNO₃) to catalyze a cation exchange that precipitates silver sulfide (Ag₂S) as an end product. This Ag₂S is rinsed three times using deionized water and ammonium hydroxide, centrifuged, and dried at 50 °C. The dry Ag₂S powder is then homogenized, with ~400 µg analyzed for $^{34}\text{S}/^{32}\text{S}$ after combustion via a Delta (V+) isotope ratio mass spectrometer (IRMS; analyte SO₂) coupled with a Costech ECS4010 Elemental Analyzer under continuous He flow. Sulfur isotope composition is expressed in standard delta notation as per mil (‰) deviations from Vienna Canyon Diablo Troilite. Ag₂S reference materials

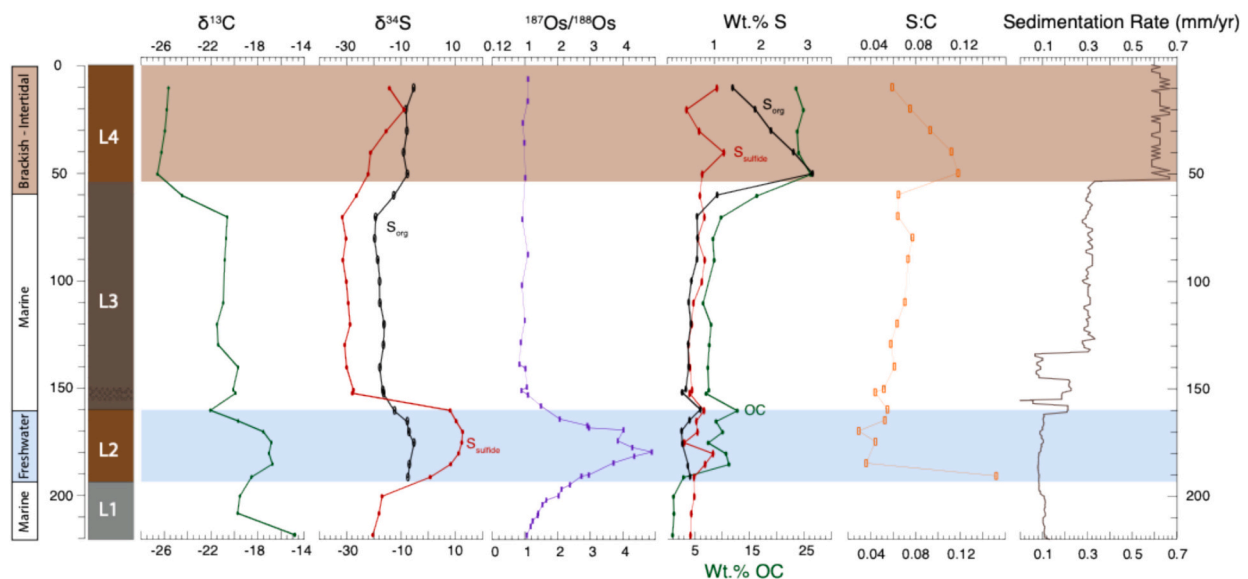


Fig. 4. Core lithofacies (L1 – L4; bottom to top) and associated geochemical analyses for Loch Duart. Left to right: isotopic values for organic carbon ($\delta^{13}C_{\text{org}}$), sulfide sulfur ($\delta^{34}S_{\text{sulfide}}$, red), organic sulfur ($\delta^{34}S_{\text{org}}$, black), and osmium ($^{187}\text{Os}/^{188}\text{Os}$; Taylor et al., 2024); weight percent values for sulfide (red), organic sulfur (black), and organic carbon (green); and the sulfur to carbon ratio (gold). Note major isotopic excursions at lithofacies boundaries associated with change in RSL modulating marine influence. Brackish – intertidal L4 preserves major shift in elemental weight percent values associated with increased accumulation of organic carbon. Sedimentation rate (mm/yr) estimated from Carbon-isotope chronology (Taylor et al., 2024). (For interpretation of the references to colour in this figure legend, the reader is referred to the web version of this article.)

were used for isotopic analyses of organic S and sulfide samples, they include IAEA-S1 (-0.3‰), IAEA-S2 ($+22.62\text{‰}$), IAEA-S3 (-32.49‰) as reported in Brand et al. (2014), alongside another in-house sulfanilamide standard. The average standard deviation (1σ) of duplicate standard $\delta^{34}\text{S}$ values is $<0.5\text{‰}$ ($n = 13$). The average standard deviation was $<0.6\text{‰}$ for sulfide CRS sample duplicates ($n = 3$) and $<1.0\text{‰}$ for organic S sample duplicates ($n = 3$).

The organic S fraction was analyzed by measuring the $\delta^{34}\text{S}$ and wt%S of the residual sediment, following the attempted extraction of S_{el} , AVS, and CRS, on the EA-IRMS as described for the sulfide fraction, above.

Total CRS-extracted sulfide concentrations have been estimated for each sample via spectrophotometric analysis. Moving forward, we refer to “sulfide” measurements as including all sulfide “pyrite-plus” phases captured during CRS. A well plate colorimetric assay (Cline, 1969) reacts each ZnS sample with diamine to form leucomethylene blue, which is a faintly colored intermediate compound. To facilitate spectrophotometric analysis, leucomethylene blue is oxidized to methylene blue ($\lambda_{\text{max}} = 664\text{ nm}$) using an Fe(III) solution. The absorbance of methylene blue is proportional to the total dissolved sulfide concentration.

3. Results

The litho-, bio-, and chemostratigraphy in LDM 20-JT preserve a local record interpreted to be driven by changes in RSL (Hamilton et al., 2015; Taylor et al., 2024). This change between marine and freshwater dominance results from the interplay between glacioeustatic sea-level rise and the effects of isostatic rebound. Both mechanisms control Loch Duart’s degree of connectivity with the ocean, and thus modulate the ecology, patterns of sedimentation, and local geochemistry that collectively define the different lithofacies identified in the core (Figs. 4 and 5).

Detailed descriptions of the lithofacies have been previously presented (Hamilton et al., 2015; Taylor et al., 2024). In brief, they include: *Lithofacies 1* (L1: 220–193 cm), a marine facies of pale grey silty clay that is conformably overlain by *Lithofacies 2* (L2: 193–160 cm), a freshwater facies that is dark brown, organic-rich silty clay with abundant rootlets. The latter is conformably overlain by *Lithofacies 3* (L3: 160–55 cm), a

marine facies of dark grey silty clay with a conspicuous layer of clasts and fragmented shells (from 155 to 145 cm) that are up to 3 cm in diameter. This lithofacies includes a hiatus in sedimentation of ~ 5 kyr between 158 and 154.5 cm (Taylor et al., 2024). Lithofacies 3 is conformably overlain by the uppermost *Lithofacies 4* (L4: 55–0 cm), a tidal marsh facies characterized by fine-grained organic carbon-rich deposits with abundant rootlets, silt, and clay material.

3.1. Sulfur analyses ($\delta^{34}\text{S}_{\text{org, sulfide}}$ wt% $S_{\text{org, sulfide}}$)

Measured parameters related to the local S system ($\delta^{34}\text{S}_{\text{sulfide}}$ and $\delta^{34}\text{S}_{\text{org}}$ wt% S_{sulfide} and S_{org}) are associated with changes in lithology and the environment at Loch Duart (Fig. 4). Moving upsection the following is observed:

Basal marine facies (L1) preserve $\delta^{34}\text{S}_{\text{sulfide}}$ values that become slightly more positive upsection (-20 to -17‰); notably, no $\delta^{34}\text{S}_{\text{org}}$ data were recovered as the organic S-phase was below the detection limit.

Freshwater facies (L2) is characterized by parabolic $\delta^{34}\text{S}$ profiles with broad peaks wherein the relationship between the three S-isotope records changes. The $\delta^{34}\text{S}_{\text{org}}$ and $\delta^{34}\text{S}_{\text{sulfide}}$ records peak at -7 and $+13\text{‰}$, respectively, during the positive excursion maxima before trending toward lower values at the top of this unit.

Middle marine facies (L3) records a large negative $\delta^{34}\text{S}_{\text{sulfide}}$ shift near its base (from $+8$ to -28‰). Over this same time interval, the organic fraction experiences a considerably lower magnitude shift, with $\delta^{34}\text{S}_{\text{org}}$ values decreasing only from -12 to -16‰ .

Uppermost tidal marsh facies (L4) records a second positive shift for both S-phases, with $\delta^{34}\text{S}_{\text{sulfide}}$ rising from -32 to -9‰ , and $\delta^{34}\text{S}_{\text{org}}$ values increasing from -19 to -5‰ .

3.2. Carbon analyses ($\delta^{13}\text{C}_{\text{org}}$, wt% TOC) & Osmium isotope record

The $\delta^{13}\text{C}_{\text{org}}$ and wt% TOC results have been previously described in detail for each lithofacies (Taylor et al., 2024). Each unit (L1 through L4) possesses a distinct carbon isotope and wt% TOC profile (Fig. 4). As with the carbon analyses, the osmium isotope ($^{187}\text{Os}/^{188}\text{Os}$) record (Fig. 4) has been described in detail (Taylor et al., 2024).

4. Discussion

4.1. Interpreting changes in the sedimentary $\delta^{34}\text{S}$ record

The sedimentary $\delta^{34}\text{S}_{\text{sulfide}}$ record at Loch Duart aligns with the environmental shifts interpreted via litho- and biostratigraphic changes (Hamilton et al., 2015; Taylor et al., 2024) and the osmium isotope record (). These environmental shifts have been interpreted as a function of variable RSL modulating the influence of marine waters at Loch Duart. Thus, the relationship between facies change and the S-isotope record is likely driven by changes in RSL via fluctuating local connectivity to the marine sulfate reservoir (Fig. 5).

The relatively stable and low $\delta^{34}\text{S}_{\text{sulfide}}$ values preserved in L1 and L3 (Fig. 5) suggest that these facies were deposited during intervals of high RSL in a system well connected to marine waters, where sulfate concentrations were high and approached modern levels ($\sim 28\text{ mM}$). Increased sulfate availability in the basin enables a more pronounced expression of the S isotope difference between sulfide preserved in the sediments and the residual water column sulfate pool. Two factors contribute to this result. First, the magnitude of the KIE resulting from MSR (ϵ_{msr}) is not reduced because of low sulfate concentrations (Habicht et al., 2002). Second, the fraction of sulfate remaining (f) decreases at a comparatively slow rate due to the high sulfate levels in the system (Fig. 2). This slows the rate at which the S isotope composition of sulfate and dissolved sulfide shifts to higher values with increasing depth in the sediment column (Fig. 3a), ultimately reducing the impact of the reservoir effect.

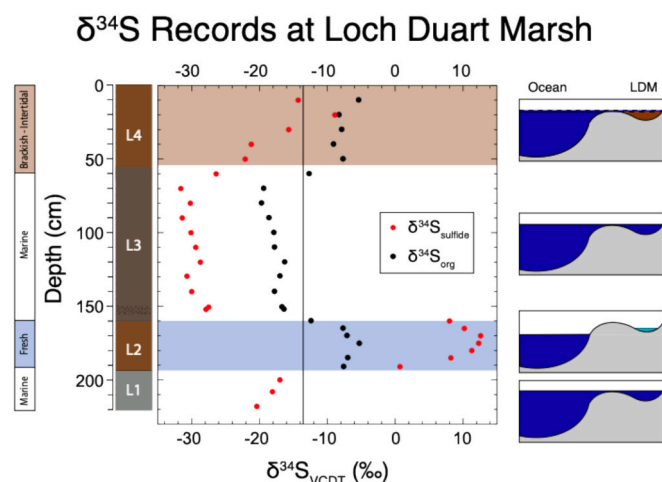


Fig. 5. Left: Isotopic values for sulfide sulfur ($\delta^{34}\text{S}_{\text{sulfide}}$, red) and organic sulfur ($\delta^{34}\text{S}_{\text{org}}$, black) through the Loch Duart sediment core. Right: A cartoon depicting changes in the hydrography of Loch Duart due to changes in eustatic sea level and isostatic rebound discussed in text. L1 and L3 depict marine waters (dark blue) high enough to completely infiltrate the study site, while L2 depicts a RSL low enough that LDM becomes fresh (light blue). L4 depicts the ephemeral connection (dashed line) between the ocean and LDM, creating a brackish (brown) local environment. (For interpretation of the references to colour in this figure legend, the reader is referred to the web version of this article.)

In contrast to L1 and L3, the comparatively high $\delta^{34}\text{S}_{\text{sulfide}}$ values preserved in L2 and L4 are consistent with systems characterized by relatively low sulfate concentrations. This reflects deposition during periods of low RSL. We believe that RSL was low enough in L2 that the basin became completely isolated with diminished or nonexistent sulfate replenishment from seawater. In L4, we believe that marine sulfate replenishment becomes restricted to high tide and that the reservoir effect was further enhanced by an increased sedimentation rate. Thus, despite some differences in depositional setting, both L2 and L4 are marked by decreased sulfate availability in the MSR-zone; this would have reduced the S isotope difference between sulfide preserved in the sediments and the residual water column sulfate reservoir. Since precise sulfate concentrations are unknown for the L2 and L4 systems, it is difficult to ascertain if ϵ_{msr} was reduced due to low sulfate concentrations. However, if we assume rates of MSR were roughly consistent across all environments, the fraction of sulfate remaining (f) would have decreased more rapidly in L2 and L4 (relative to L1 and L3) due to much lower sulfate levels in the system (Fig. 2). This increases the rate at which the S isotope composition of sulfate and dissolved sulfide shift to higher values with depth in the sediments (Fig. 3b, c), thereby enhancing the impact of the reservoir effect.

The conclusions above align with the findings of Taylor et al. (2023), who determined that the L1-L2 transition marked a shift from a marine to a relatively freshwater environment as glacio-isostatic rebound outpaced the background eustatic rise (i.e., RSL fall). This interpretation is supported by the coincident radiogenic $^{187}\text{Os}/^{188}\text{Os}$ compositions, which likely reflect the weathering of terrestrial materials (e.g., biotite; Taylor et al., 2024) present in the Lewisian gneiss bedrock surrounding Loch Duart (Burton et al., 2000). Taylor et al. (2024) also quantified a marked increase in sedimentation rate in L4.

The S isotope record across the L1-L2-L3 transitions, particularly the relationship between changes in $\delta^{34}\text{S}_{\text{sulfide}}$ and $\delta^{34}\text{S}_{\text{org}}$, warrants further attention. As discussed above, the decrease in sulfate availability across the L1-L2 transition would have pushed the S isotope composition of the residual pore water sulfate pool to progressively higher values, resulting in the formation of ^{34}S -enriched dissolved sulfide. A portion of this dissolved sulfide could then react with available iron, if present, to form pyrite with essentially the same isotope composition as the dissolved sulfide. However, a separate fraction of the MSR-generated ^{34}S -enriched dissolved sulfide (and associated intermediate S species) could facilitate OM sulfurization, generating $\delta^{34}\text{S}_{\text{org}}$ values that are ^{34}S -enriched relative to the dissolved sulfide (Fig. 3). Indeed, an increase in TOC (up to $\sim 10\%$; Fig. 4) coincides with the appearance of measurable organic S. Interestingly, the $\delta^{34}\text{S}_{\text{org}}$ values in L2 are lower than the coexisting $\delta^{34}\text{S}_{\text{pyrite}}$ values (represented by $\delta^{34}\text{S}_{\text{sulfide}}$ on Figs. 3, 4 and 5). As mentioned above, this situation is unusual, with only a few instances of ^{34}S -enrichment of S_{org} documented in the literature, none exhibiting a coherent excursion as reported here.

We hypothesize that this reversal in $\delta^{34}\text{S}$ values ($\delta^{34}\text{S}_{\text{org}} < \delta^{34}\text{S}_{\text{sulfide}}$) in L2 may arise from a spatial decoupling of pyrite and organic S formation within the water column and/or sediments, amplified by the reservoir effect in a low-sulfate system. In systems with well-oxygenated bottom waters, dissolved sulfide generation via MSR is restricted to the anoxic portions of the sediments. This MSR-generated dissolved sulfide may then react with iron to form pyrite (with a $\delta^{34}\text{S}$ value equivalent to that of the dissolved sulfide at the depth of formation) and/or be utilized during OM sulfurization (with a $\delta^{34}\text{S}_{\text{org}}$ value that is ^{34}S -enriched relative to that of the dissolved sulfide at the depth of OM sulfurization) (Fig. 3a). Importantly, the S isotope composition of pyrite and S_{org} ultimately preserved represent depth-integrated, average $\delta^{34}\text{S}$ values. Therefore, because the S isotope composition of dissolved sulfide evolves to increasingly ^{34}S -enriched values with depth in the sediments, the precise location of pyrite formation in relation to OM sulfurization significantly affects the average $\delta^{34}\text{S}_{\text{sulfide}}$ and $\delta^{34}\text{S}_{\text{org}}$ values ultimately preserved in the sedimentary record.

For example, if OM sulfurization primarily occurred in the upper

portion of the sediments where the organic C is relatively labile and the S isotope composition of dissolved sulfide is ^{34}S -depleted (relative to deeper sediments), the average $\delta^{34}\text{S}$ value of sulfidized OM would also be ^{34}S -depleted (although somewhat ^{34}S -enriched compared to the dissolved sulfide). Moreover, if pyrite formation occurred primarily in the deeper portions of the sediment column (perhaps due to the reactivity of the iron reservoir), then the average $\delta^{34}\text{S}_{\text{sulfide}}$ value may be ^{34}S -enriched relative to the $\delta^{34}\text{S}_{\text{org}}$ values formed higher in the sediment column (Fig. 3b). This holds particular importance in a low sulfate system as the rate of $\delta^{34}\text{S}$ change with depth of MSR-generated dissolved sulfide is greater compared to a high sulfate system (compare Fig. 3a and b). These conditions, combined with the relatively short reaction time for OM sulfurization, could explain how $\delta^{34}\text{S}_{\text{org}}$ in L2 is maintained at relatively low values compared with coeval $\delta^{34}\text{S}_{\text{sulfide}}$, which reflects iron sulfidation in deeper sections of the sediment column.

This effect may be even more pronounced if the chemocline shifts upward into the water column of a low sulfate system, allowing sulfide generation via MSR to proceed in an anoxic water column (Fig. 3c). In fact, X-ray fluorescence analysis reveals broad peaks in selenium (Se) and copper (Cu) at 182 cm, coinciding with the main peak in $^{187}\text{Os}/^{188}\text{Os}$ within L2 (Taylor et al., 2024). In solution, copper complexes with OM; thus, increased OM is often associated with an accumulation of copper (Tribouillard et al., 2006). In a reducing environment, particularly one capable of facilitating MSR, Cu(II) is reduced to Cu(I) (Tribouillard et al., 2006). Thus, copper accumulation in marine or lacustrine sediments is also associated with anoxic conditions. Selenium, another redox-sensitive metal, serves as another potential indicator of anoxia (Tolu et al., 2014; Wen et al., 2014), especially when found in high quantities alongside significant levels of preserved OM. Together, these geochemical observations suggest that L2 may have been characterized by anoxic bottom water conditions, which could partly explain the distinct S-isotope record. However, water column anoxia is not required to generate the S isotope record presented here.

Alternatively, the observed S isotopic relationship between sulfide and Sorg ($\delta^{34}\text{S}_{\text{org}} < \delta^{34}\text{S}_{\text{sulfide}}$) may have resulted from the addition of terrestrial organic S. We investigated $\delta^{34}\text{S}$ records of terrestrial plants, which appear to closely track the $\delta^{34}\text{S}$ values of the local source of soil sulfate (Kaplan and Rittenberg, 1964) with upwards of a -2% fractionation effect measured during assimilation (Cavallaro et al., 2022). A robust compilation of terrestrial plant S-isotope measurements from locations across the USSR exhibits $\delta^{34}\text{S}$ values ranging from -7% to $+19\%$, reflecting differences in the S-isotopic composition of local rainwater (Chukhrov et al., 1980). Additionally, *Sphagnum* moss in a remote bog on the Isle of Mull (Scotland, UK) exhibits a range in $\delta^{34}\text{S}$ values ($+5.4$ to $+18.7\%$) (Bottrell and Novak, 1997). The more positive $\delta^{34}\text{S}$ values are shown to be associated with chloride and are thus interpreted as approximating ocean spray during winter storms, while the more ^{34}S -depleted values are considered to represent anthropogenic pollution of rainwater during the summer months. As such, the range of potential $\delta^{34}\text{S}$ values for terrestrial plants suggests that it is unlikely that an augmented terrestrial OM supply could account for the $\delta^{34}\text{S}_{\text{org}}$ record in L2 (-12 to -7%) at Loch Duart.

Lithofacies 3 is characterized by a renewed connection to the marine sulfate reservoir and trace metal abundances suggest reoxygenation. Reventilated bottom waters and replenished $[\text{SO}_4^{2-}]$ would have returned the basin to normal marine conditions, as evidenced by relatively stable and low $\delta^{34}\text{S}_{\text{sulfide}}$ values that remain systematically more negative than concurrent $\delta^{34}\text{S}_{\text{org}}$.

Lithofacies 4 is associated with a fall in RSL and a positive $\delta^{34}\text{S}_{\text{sulfide}}$ shift. Today, Loch Duart is only inundated by seawater at high tide (Taylor et al., 2024). However, osmium isotopes still reflect sufficient marine inundation to maintain values very close to modern seawater. Sedimentation rates at Loch Duart increase by 100% at the L3 – L4 boundary (Fig. 4; Taylor et al., 2024) and are accompanied by a substantial increase in TOC (from 16 to 25%) and weight % organic S (from

1 to 3 %). While these two parameters covary, we hypothesize that the noticeably larger relative increase in the weight % of organic S, coupled with the subsequent steady decrease up section, could be explained by diagenetic accumulation in the sediment pore space. This would halve the duration during which pore-space MSR could interact with the overlying sulfate reservoir. We propose that this quasi-restriction from the seawater sulfate reservoir may partly be responsible for the positive $\delta^{34}\text{S}$ excursions in both sulfide and S_{org} , reflecting a distillation effect similar to—but smaller than—the one observed in L2. This excursion is thus comparable to another study examining changes in $\delta^{34}\text{S}$ associated with glacial-interglacial cycles in the Mediterranean (Pasquier et al., 2017). Notably, $\delta^{34}\text{S}$ values in L4 do not approach those recorded in the completely restricted freshwater phase of L2. This discrepancy may be explained either by the rejuvenation of the local sulfate reservoir through the inundation of seawater during high tide or by the relatively young age of the sediments, which has not yet permitted the full expression of later-stage diagenesis.

4.2. Sulfur and osmium isotopic comparison

The osmium isotope record at Loch Duart can be used to reconstruct the history of marine influence in the basin. Taylor et al. (2024) illustrate this by comparing a $^{187}\text{Os}/^{188}\text{Os}$ profile with foraminiferal data in conjunction with diatom records (Hamilton et al., 2015), finding that radiogenic $^{187}\text{Os}/^{188}\text{Os}$ values are associated with the freshwater L2 facies (1.33–4.89). Given this relationship, we compare the osmium

isotope record with our own $\delta^{34}\text{S}_{\text{sulfide}}$ data to evaluate the extent to which they may or may not be mutually supportive (Fig. 6). Shifts in osmium isotope composition at Loch Duart are driven by the degree of marine influence (Taylor et al., 2024). The $^{187}\text{Os}/^{188}\text{Os}$ values that are more radiogenic than 1.06 represent increased terrestrial influence and diminished marine inundation/connectivity. Our data suggest that $\delta^{34}\text{S}_{\text{sulfide}}$ values are modulated mainly by $[\text{SO}_4^{2-}]$, a function of the degree of connectivity to the marine sulfate reservoir. Fig. 6 demonstrates that the relationship between the two isotopic systems behaves as predicted: radiogenic, freshwater $^{187}\text{Os}/^{188}\text{Os}$ values are associated with higher $\delta^{34}\text{S}_{\text{sulfide}}$ values, whereas marine $^{187}\text{Os}/^{188}\text{Os}$ values are linked to lower $\delta^{34}\text{S}_{\text{sulfide}}$ values, and brackish conditions correlate with osmium and $\delta^{34}\text{S}_{\text{sulfide}}$ values that fall in between the two end members.

The relationship between these two datasets supports the interpretations stated for each geochemical proxy: the Os isotope proxy is a valuable tool for establishing marine connection in near coastal environments, and $\delta^{34}\text{S}$ can similarly be utilized in low-sulfate environments to identify marine incursions. Given that these isotopic profiles are driven by the same fundamental mechanism (changes in RSL and thus ocean connectivity), their mutual profiles provide a fine-tuned geochemical history of Loch Duart (Fig. 6). The stratigraphic position of each data point within the Os- $\delta^{34}\text{S}$ space (with 1 representing the deepest point in the core at 218 cm, 2 representing the next deepest at 208 cm, etc.) opens a geochemical window into the environmental evolution of the system that can be tracked across the various lithofacies. Consequently, these results suggest that S isotopes, along with osmium

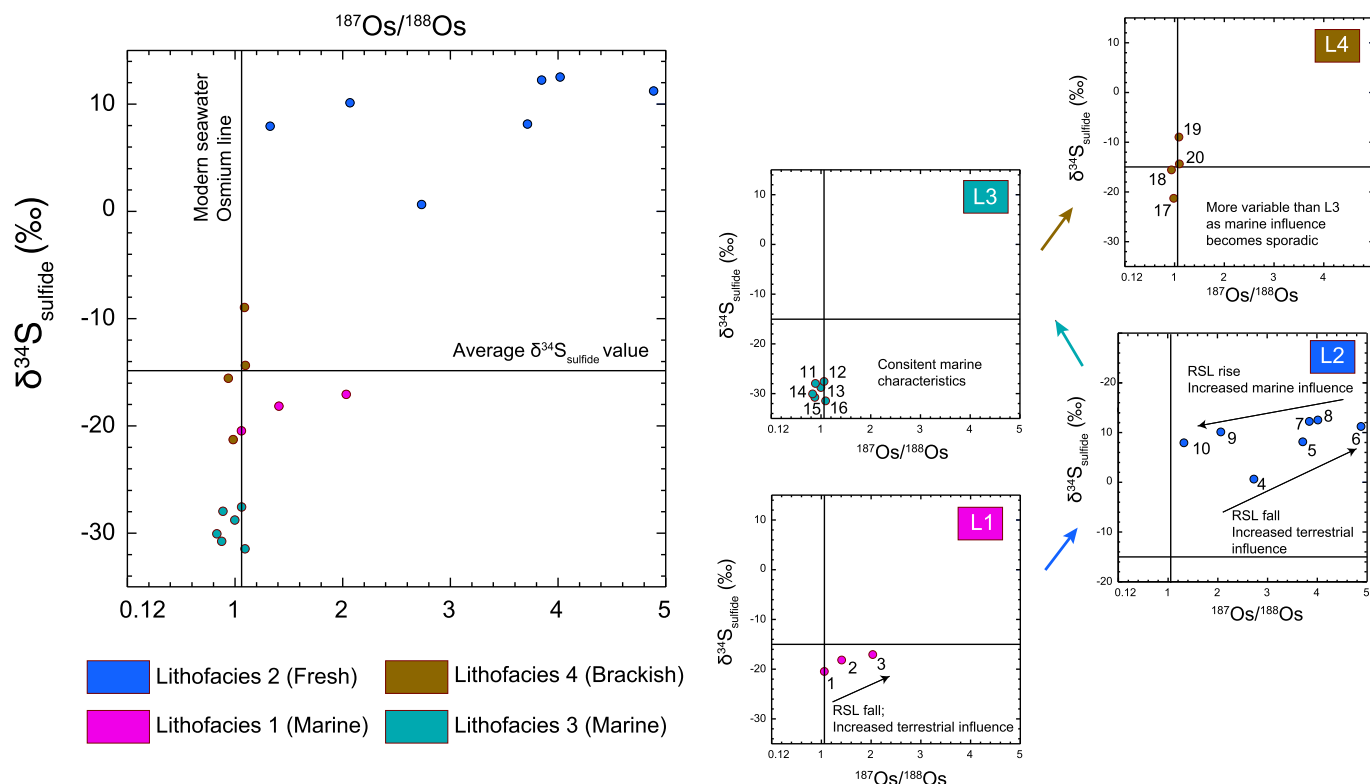


Fig. 6. Top: $\delta^{34}\text{S}_{\text{sulfide}}$ (average = -14.7 ‰) plotted against $^{187}\text{Os}/^{188}\text{Os}$ (Marine values ~ 1.06).

Right: Individual lithofacies subsets L1 (Pink; marine), L2 (Blue, fresh water), L3 (Green, marine), L4 (Brown, brackish); numbers depict successive stratigraphic height within each lithofacies with 1 = bottommost data point. L1 preserves distinct increase in both $\delta^{34}\text{S}_{\text{pyr}}$ and $^{187}\text{Os}/^{188}\text{Os}$ interpreted to reflect falling RSL and decreasing marine influence. An abrupt shift in L2 (note: change in the range of the y-axis) records a dramatic change in the depositional setting. The lower portion of the facies experiences a progressive “climb” in both isotopic signals, presumably a reflection of continued RSL fall, followed by a subsequent “fall” in these signals as measurements of both $^{187}\text{Os}/^{188}\text{Os}$ and $\delta^{34}\text{S}_{\text{sulfide}}$ trend back toward more normal marine values. A major shift in L3 records return to stable, marine conditions. L4 preserves $^{187}\text{Os}/^{188}\text{Os}$ values slightly higher, but still very similar to those in L3 alongside a much more significant shift in $\delta^{34}\text{S}_{\text{sulfide}}$ values. The $^{187}\text{Os}/^{188}\text{Os}$ signature can be explained by high-tide marine inundation continuing to supply a sufficient marine derived $^{187}\text{Os}/^{188}\text{Os}$ composition to the water column. We hypothesize that the shift in $\delta^{34}\text{S}_{\text{sulfide}}$ values might be largely due to an increase in sedimentation rate (Taylor et al., 2024), creating a distillation effect. (For interpretation of the references to colour in this figure legend, the reader is referred to the web version of this article.)

isotopes, have the potential to reconstruct environmental changes associated with RSL change.

5. Conclusions

The sediment core recovered at Loch Duart preserves an exceptional archive of environmental change since the Late Glacial period with a robust suite of bio-, litho-, and chemostratigraphic records suggesting that fluctuating RSL, driven by the interplay of eustatic sea level rise and isostatic rebound, caused changes in the depositional environment over the last ~17 kyrs. The sedimentary record preserves four distinct lithofacies that document variability in marine influence.

The osmium record (Taylor et al., 2024) was utilized as a proxy for marine inundation into the basin, with more radiogenic $^{187}\text{Os}/^{188}\text{Os}$ values (>1.06) reflecting terrestrial influence. Comparing the Loch Duart $^{187}\text{Os}/^{188}\text{Os}$ values to our $\delta^{34}\text{S}$ record (Fig. 6) demonstrates a strong covariance between the two datasets, providing robust evidence that RSL change is the driving mechanism for both geochemical signals.

The $\delta^{34}\text{S}_{\text{sulfide}}$ record fits coherently within the established paleo-environmental history of Loch Duart, which has been defined by changes in biotic assemblages (Hamilton et al., 2015; Taylor et al., 2024). Relatively stable and low $\delta^{34}\text{S}_{\text{sulfide}}$ values are observed in marine facies (L1 and L3), while marked positive $\delta^{34}\text{S}$ excursions are preserved in sediments deposited under fresh (L2) and brackish water (L4) conditions, which we primarily interpret as a function of decreased local sulfate concentrations due to isolation from the seawater sulfate reservoir.

Lithofacies 2 preserves a novel $\delta^{34}\text{S}$ profile characterized by ^{34}S -depleted organic S relative to coeval pyrite. This finding is unusual in the geologic record, as the parameters surrounding organic matter sulfuration tend to produce $\delta^{34}\text{S}_{\text{org}} \sim 10\text{‰}$ heavier than coincident pyrite (e.g. Anderson and Pratt, 1995). To our knowledge, previous studies that have recorded a similar inversion ($\delta^{34}\text{S}_{\text{org}} < \delta^{34}\text{S}_{\text{sulfide}}$), have only observed isolated, individual data points nested within sections preserving the more typical relationship ($\delta^{34}\text{S}_{\text{org}} > \delta^{34}\text{S}_{\text{sulfide}}$) and have interpreted these signals to reflect the diachronous formation of the two S-phases (e.g., Raven et al., 2015, 2023). These single data point observations contrast starkly with the record at Loch Duart, which preserves a succession of six data points spanning the entire freshwater facies (L2; 31 cm), directly overlapping with the positive S isotope excursion. We suggest that this inverse relationship ($\delta^{34}\text{S}_{\text{org}} < \delta^{34}\text{S}_{\text{sulfide}}$) may indicate that the predominant zone of OM sulfuration occurs higher within the water column and/or sediments than the primary zone of pyrite formation, in a system with low sulfate concentrations. As a result, the S isotopic composition of the dissolved sulfide responsible for pyrite formation is ^{34}S -enriched relative to the dissolved sulfide utilized during the OM sulfuration process. While more work is needed to test this hypothesis, this inverse relationship may serve as an additional diagnostic tool for identifying low-sulfate systems in the geologic past.

CRedit authorship contribution statement

L.G. Podrecca: Writing – review & editing, Writing – original draft, Visualization, Validation, Project administration, Methodology, Investigation, Formal analysis, Data curation, Conceptualization. **A.L. Masterson:** Writing – review & editing, Visualization, Supervision, Methodology, Investigation, Formal analysis, Data curation, Conceptualization. **M.T. Hurtgen:** Writing – review & editing, Visualization, Supervision, Conceptualization. **J. Taylor:** Writing – review & editing, Resources, Investigation, Data curation. **J.M. Lloyd:** Writing – review & editing, Resources. **D. Selby:** Writing – review & editing, Resources, Project administration, Funding acquisition. **B.B. Sageman:** Writing – review & editing, Supervision, Resources, Project administration, Funding acquisition, Conceptualization.

Declaration of competing interest

The authors declare that they have no known competing financial interests or personal relationships that could have appeared to influence the work reported in this paper.

Data availability

Data will be made available on request.

Acknowledgements

We thank Neil Tunstall, Chris Longley, Chris Ottley, and Geoff Nowell from Durham University (UK) for their analytical support. Jennifer Taylor acknowledges support from the Durham Doctoral Scholarship.

References

- Amrani, A., Ma, Q., Ahmad, W.S., Aizenshtat, Z., Tang, Y., 2008. Sulfur isotope fractionation during incorporation of sulfur nucleophiles into organic compounds. *Chem. Commun.* 1356. <https://doi.org/10.1039/b717113g>.
- Anderson, T.F., Pratt, L.M., 1995. Isotopic evidence for the origin of organic sulfur and elemental sulfur in marine sediments. <https://doi.org/10.1021/bk-1995-0612.ch021>.
- Bak, F., Cypionka, H., 1987. A novel type of energy metabolism involving fermentation of inorganic sulphur compounds. *Nature* 326 (6116), 891–892. <https://doi.org/10.1038/326891a0>.
- Berner, R.A., 1989. Biogeochemical cycles of carbon and sulfur and their effect on atmospheric oxygen over phanerozoic time. *Glob. Planet. Chang.* 1, 97–122. [https://doi.org/10.1016/0921-8181\(89\)90018-0](https://doi.org/10.1016/0921-8181(89)90018-0).
- Berner, R.A., Raiswell, R., 1983. Burial of organic carbon and pyrite sulfur in sediments over phanerozoic time: a new theory. *Geochim. Cosmochim. Acta* 47, 855–862. [https://doi.org/10.1016/0016-7037\(83\)90151-5](https://doi.org/10.1016/0016-7037(83)90151-5).
- Bottrell, S., Novak, M., 1997. Sulphur isotopic study of two pristine Sphagnum bogs in the Western British Isles. *J. Ecol.* 85, 125. <https://doi.org/10.2307/2960644>.
- Bradley, A.S., Leavitt, W.D., Schmidt, M., Knoll, A.H., Girguis, P.R., Johnston, D.T., 2016. Patterns of sulfur isotope fractionation during microbial sulfate reduction. *Geobiology* 14 (1), 91–101. <https://doi.org/10.1111/gbi.12149>.
- Brand, W.A., Coplen, T.B., Vogl, J., Rosner, M., Prohaska, T., 2014. Assessment of international reference materials for isotope-ratio analysis (IUPAC Technical Report). *Pure Appl. Chem.* 86 (3), 425–467. <https://doi.org/10.1515/pac-2013-1023>.
- Brüchert, V., Pratt, L.M., 1996. Contemporaneous early diagenetic formation of organic and inorganic sulfur in estuarine sediments from St. Andrew Bay, Florida, USA. *Geochim. Cosmochim. Acta* 60, 2325–2332. [https://doi.org/10.1016/0016-7037\(96\)00087-7](https://doi.org/10.1016/0016-7037(96)00087-7).
- Brunner, B., Bernasconi, S.M., 2005. A revised isotope fractionation model for dissimilatory sulfate reduction in sulfate reducing bacteria. *Geochim. Cosmochim. Acta* 69 (20), 4759–4771. <https://doi.org/10.1016/j.gca.2005.04.015>.
- Burton, K.W., Capmas, F., Birck, J.-L., Allègre, C.J., Cohen, A.S., 2000. Resolving crystallisation ages of Archean mafic-ultramafic rocks using the Re–Os isotope system. *Earth Planet. Sci. Lett.* 179, 453–467. [https://doi.org/10.1016/S0012-821X\(00\)00134-5](https://doi.org/10.1016/S0012-821X(00)00134-5).
- Canfield, D.E., 1998. A new model for Proterozoic ocean chemistry. *Nature* 396, 450–453. <https://doi.org/10.1038/24839>.
- Canfield, D.E., 2001. Biogeochemistry of Sulfur Isotopes. *Rev. Mineral. Geochem.* 43, 607–636. <https://doi.org/10.2138/gsrmg.43.1.607>.
- Canfield, D.E., Raiswell, R., 1999. The evolution of the sulfur cycle. *Am. J. Sci.* 299, 697–723.
- Canfield, D.E., Teske, A., 1996. Late Proterozoic rise in atmospheric oxygen concentration inferred from phylogenetic and Sulphur-isotope studies. *Nature* 382, 127–132. <https://doi.org/10.1038/382127a0>.
- Canfield, D.E., Raiswell, R., Westrich, J.T., Reaves, C.M., Berner, R.A., 1986. The use of chromium reduction in the analysis of reduced inorganic sulfur in sediments and shales. *Chem. Geol.* 54 (1–2), 149–155. [https://doi.org/10.1016/0009-2541\(86\)90078-1](https://doi.org/10.1016/0009-2541(86)90078-1).
- Cavallaro, V., Maghrebi, M., Caschetto, M., Sacchi, G.A., Nocito, F.F., 2022. Sulfur stable isotope discrimination in rice: a sulfur isotope mass balance study. *Front. Plant Sci.* 13, 837517. <https://doi.org/10.3389/fpls.2022.837517>.
- Chukhrov, F.V., Ermilova, L.P., Churikov, V.S., Nosik, L.P., 1980. The isotopic composition of plant sulfur. *Org. Geochem.* 2, 69–75. [https://doi.org/10.1016/0146-6380\(80\)90022-4](https://doi.org/10.1016/0146-6380(80)90022-4).
- Claypool, G.E., 2004. Ventilation of marine sediments indicated by depth profiles of pore water sulfate and $\delta^{34}\text{S}$. In: *The Geochemical Society Special Publications*, vol. 9. Elsevier, pp. 59–65. [https://doi.org/10.1016/S1873-9881\(04\)80007-5](https://doi.org/10.1016/S1873-9881(04)80007-5).
- Cline, J.D., 1969. Spectrophotometric determination of hydrogen sulfide in natural waters 1. *Limnol. Oceanogr.* 14, 454–458. <https://doi.org/10.4319/lo.1969.14.3.0454>.

- Crowe, S.A., Paris, G., Katsev, S., Jones, C., Kim, S.-T., Zerkle, A.L., Nomosatryo, S., Fowle, D.A., Adkins, J.F., Sessions, A.L., Farquhar, J., Canfield, D.E., 2014. Sulfate was a trace constituent of Archean seawater. *Science* 346 (6210), 735–739. <https://doi.org/10.1126/science.1258168>.
- Fike, D.A., Bradley, A.S., Rose, C.V., 2015. Rethinking the ancient sulfur cycle. *Annu. Rev. Earth Planet. Sci.* 43, 593–622. <https://doi.org/10.1146/annurev-earth-060313-054802>.
- Friedrich, C.G., Rother, D., Bardischewsky, F., Quentmeier, A., Fischer, J., 2001. Oxidation of reduced inorganic sulfur compounds by bacteria: emergence of a common mechanism? *Appl. Environ. Microbiol.* 67, 2873–2882. <https://doi.org/10.1128/AEM.67.7.2873-2882.2001>.
- Friedrich, C.G., Bardischewsky, F., Rother, D., Quentmeier, A., Fischer, J., 2005. Prokaryotic sulfur oxidation. *Curr. Opin. Microbiol.* 8, 253–259. <https://doi.org/10.1016/j.mib.2005.04.005>.
- Gautier, D.L., 1986. Cretaceous shales from the western interior of North America: sulfur/carbon ratios and sulfur-isotope composition. *Geology* 14 (3), 225–228. [https://doi.org/10.1130/0091-7613\(1986\)14%3C225:CSFTW1%3E2.0.CO;2](https://doi.org/10.1130/0091-7613(1986)14%3C225:CSFTW1%3E2.0.CO;2).
- Goldhaber, M.B., Kaplan, I.R., 1975. Controls and consequences of sulfate reduction rates in recent marine sediments. *Soil Science* 119 (1), 42–55.
- Goldhaber, M.B., Kaplan, I.R., 1980. Mechanisms of sulfur incorporation and isotope fractionation during early diagenesis in sediments of the Gulf of California. *Mar. Chem.* 9 (2), 95–143. [https://doi.org/10.1016/0304-4203\(80\)90063-8](https://doi.org/10.1016/0304-4203(80)90063-8).
- Gomes, M.L., Hurtgen, M.T., 2013. Sulfur isotope systematics of a euxinic, low-sulfate lake: evaluating the importance of the reservoir effect in modern and ancient oceans. *Geology* 41 (6), 663–666. <https://doi.org/10.1130/G34187.1>.
- Gröger, J., Franke, J., Hamer, K., Schulz, H.D., 2009. Quantitative recovery of elemental sulfur and improved selectivity in a chromium-reducible sulfur distillation. *Geostand. Geoanal. Res.* 33, 17–27. <https://doi.org/10.1111/j.1751-908X.2009.00922.x>.
- Habicht, K.S., Gade, M., Thamdrup, B., Berg, P., Canfield, D.E., 2002. Calibration of sulfate levels in the Archean Ocean. *Science* 298 (5602), 2372–2374. <https://doi.org/10.1126/science.1078265>.
- Haley, I., Fike, D.A., Pasquier, V., Bryant, R.N., Wenk, C.B., Turchyn, A.V., Johnston, D.T., Claypool, G.E., 2023. Sedimentary parameters control the sulfur isotope composition of marine pyrite. *Science* 382, 946–951. <https://doi.org/10.1126/science.adh1215>.
- Hamilton, C.A., Lloyd, J.M., Barlow, N.L.M., Innes, J.B., Flecker, R., Thomas, C.P., 2015. Late Glacial to Holocene relative sea-level change in Assynt, Northwest Scotland, UK. *Quat. Res.* 84, 214–222. <https://doi.org/10.1016/j.yqres.2015.07.001>.
- Harrison, A.G., Thode, H.G., 1958. Mechanism of the bacterial reduction of sulphate from isotope fractionation studies. *Trans. Faraday Soc.* 54, 84. <https://doi.org/10.1039/tf9585400084>.
- Hartgers, W.A., López, J.F., Sinninghe Damsté, J.S., Reiss, C., Maxwell, J.R., Grimalt, J. O., 1997. Sulfur-binding in recent environments: II. Speciation of sulfur and iron and implications for the occurrence of organo-sulfur compounds. *Geochim. Cosmochim. Acta* 61, 4769–4788. [https://doi.org/10.1016/S0016-7037\(97\)00279-2](https://doi.org/10.1016/S0016-7037(97)00279-2).
- Hartnett, H.E., Keil, R.G., Hedges, J.L., Devol, A.H., 1998. Influence of oxygen exposure time on organic carbon preservation in continental margin sediments. *Nature* 391, 572–575. <https://doi.org/10.1038/35351>.
- Hemingway, J.D., Rothman, D.H., Grant, K.E., Rosengard, S.Z., Eglinton, T.I., Derry, L.A., Galy, V.V., 2019. Mineral protection regulates long-term global preservation of natural organic carbon. *Nature* 570, 228–231. <https://doi.org/10.1038/s41586-019-1280-6>.
- Holland, H.D., 1973. Systematics of the isotope composition of sulfur in the oceans during the Phanerozoic and its implications for atmospheric oxygen. *Geochim. Cosmochim. Acta* 37, 2605–2616. [https://doi.org/10.1016/0016-7037\(73\)90268-8](https://doi.org/10.1016/0016-7037(73)90268-8).
- Holsler, W.T., Maynard, J.B., Cruikshank, K.M., 1989. Modelling the natural cycle of Sulphur through Phanerozoic time. *Evol. Global Biogeochem. Sulphur Cycle* 21–56.
- Hülse, D., Arndt, S., Ridgwell, A., 2019. Mitigation of extreme ocean anoxic event conditions by organic matter sulfurization. *Paleoceanogr. Paleoclimatology* 34, 476–489. <https://doi.org/10.1029/2018PA003470>.
- Kaplan, I.R., Rittenberg, S.C., 1964. Microbiological Fractionation of Sulphur Isotopes. *J. Gen. Microbiol.* 34, 195–212. <https://doi.org/10.1099/00221287-34-2-195>.
- Leavitt, W.D., Haley, I., Bradley, A.S., Johnston, D.T., 2013. Influence of sulfate reduction rates on the Phanerozoic sulfur isotope record. *Proc. Natl. Acad. Sci.* 110, 11244–11249. <https://doi.org/10.1073/pnas.1218874110>.
- Long, A.J., Woodroffe, S.A., Roberts, D.H., Dawson, S., 2011. Isolation basins, sea-level changes and the Holocene history of the Greenland Ice Sheet. *Quat. Sci. Rev.* 30, 3748–3768. <https://doi.org/10.1016/j.quascirev.2011.10.013>.
- Maynard, J.B., 1980. Sulfur isotopes of iron sulfides in Devonian-Mississippian shales of the Appalachian Basin: control by rate of sedimentation. *Am. J. Sci.* 280, 772–786. <https://doi.org/10.2475/ajs.280.8.772>.
- Ohmoto, H., Goldhaber, M.B., 1997. Sulfur and carbon isotopes. In: Barnes, H.L. (Ed.), *Geochemistry of Hydrothermal Ore Deposits*. John Wiley & Sons, New York, pp. 517–611.
- Pasquier, V., Sansjofre, P., Rabineau, M., Revillon, S., Houghton, J., Fike, D.A., 2017. Pyrite sulfur isotopes reveal glacial–interglacial environmental changes. *Proc. Natl. Acad. Sci.* 114, 5941–5945. <https://doi.org/10.1073/pnas.1618245114>.
- Peucker-Ehrenbrink, B., Ravizza, G., 2000. The marine osmium isotope record. *Terra Nova* 12, 205–219. <https://doi.org/10.1046/j.1365-3121.2000.00295.x>.
- Raven, M.R., Adkins, J.F., Werne, J.P., Lyons, T.W., Sessions, A.L., 2015. Sulfur isotopic composition of individual organic compounds from Cariaco Basin sediments. *Org. Geochem.* 80, 53–59. <https://doi.org/10.1016/j.orggeochem.2015.01.002>.
- Raven, M.R., Fike, D.A., Bradley, A.S., Gomes, M.L., Owens, J.D., Webb, S.A., 2019. Paired organic matter and pyrite $\delta^{34}\text{S}$ records reveal mechanisms of carbon, sulfur, and iron cycle disruption during Ocean Anoxic Event 2. *Earth Planet. Sci. Lett.* 512, 27–38. <https://doi.org/10.1016/j.epsl.2019.01.048>.
- Raven, M.R., Keil, R.G., Webb, S.M., 2021. Rapid, concurrent formation of organic sulfur and iron sulfides during experimental sulfurization of sinking marine particles. *Glob. Biogeochem. Cycles* 35 (9). <https://doi.org/10.1029/2021GB007062> p. e2021GB007062.
- Raven, M.R., Crockford, P.W., Hodgskiss, M.S.W., Lyons, T.W., Tino, C.J., Webb, S.M., 2023. Organic matter sulfurization and organic carbon burial in the Mesoproterozoic. *Geochim. Cosmochim. Acta* 347, 102–115. <https://doi.org/10.1016/j.gca.2023.02.020>.
- Rooney, A.D., Selby, D., Lloyd, J.M., Roberts, D.H., Lückge, A., Sageman, B.B., Prouty, N. G., 2016. Tracking millennial-scale Holocene glacial advance and retreat using osmium isotopes: Insights from the Greenland ice sheet. *Quat. Sci. Rev.* 138, 49–61. <https://doi.org/10.1016/j.quascirev.2016.02.021>.
- Roy, A.B., Trudinger, P.A., 1970. *The Biochemistry of Inorganic Compounds of Sulfur*. Cambridge Univ. Press, London.
- Seal, R.R., 2006. Sulfur Isotope Geochemistry of Sulfide Minerals. *Rev. Mineral. Geochem.* 61, 633–677. <https://doi.org/10.2138/rmg.2006.61.12>.
- Sharma, M., Papanastassiou, D.A., Wassburg, G.J., 1997. The concentration and isotopic composition of osmium in the oceans. *Geochim. Cosmochim. Acta* 61, 3287–3299. [https://doi.org/10.1016/S0016-7037\(97\)00210-X](https://doi.org/10.1016/S0016-7037(97)00210-X).
- Shawar, L., Halevy, I., Said-Ahmad, W., Feinstein, S., Boyko, V., Kamysny, A., Amrani, A., 2018. Dynamics of pyrite formation and organic matter sulfurization in organic-rich carbonate sediments. *Geochim. Cosmochim. Acta* 241, 219–239. <https://doi.org/10.1016/j.gca.2018.08.048>.
- Shen, Y., Buick, R., Canfield, D.E., 2001. Isotopic evidence for microbial sulphate reduction in the early Archean era. *Nature* 410, 77–81. <https://doi.org/10.1038/35065071>.
- Sim, M.S., Bosak, T., Ono, S., 2011a. Large sulfur isotope fractionation does not require disproportionation. *Science* 333, 74–77. <https://doi.org/10.1126/science.1205103>.
- Sim, M.S., Ono, S., Donovan, K., Templer, S.P., Bosak, T., 2011b. Effect of electron donors on the fractionation of sulfur isotopes by a marine *Desulfovibrio* sp. *Geochim. Cosmochim. Acta* 75, 4244–4259. <https://doi.org/10.1016/j.gca.2011.05.021>.
- Sinninghe Damsté, J.S., De Leeuw, J.W., 1990. Analysis, structure and geochemical significance of organically-bound Sulphur in the geosphere: State of the art and future research. *Org. Geochem.* 16, 1077–1101. [https://doi.org/10.1016/0146-6380\(90\)90145-P](https://doi.org/10.1016/0146-6380(90)90145-P).
- Taylor, J., Selby, D., Lloyd, J.M., Podrecca, L., Masterson, A.L., Sageman, B.B., Szidat, S., 2024. Palaeoenvironmental reconstruction of Loch Duart (NW Scotland, UK) since the Last Glacial Maximum: implications from a multiproxy approach. *J. Quat. Sci.* 39, 6–23. <https://doi.org/10.1002/jqs.3566>.
- Tolu, J., Thiry, Y., Bueno, M., Jolivet, C., Potin-Gautier, M., Le Hécho, I., 2014. Distribution and speciation of ambient selenium in contrasted soils, from mineral to organic rich. *Sci. Total Environ.* 479–480, 93–101. <https://doi.org/10.1016/j.scitotenv.2014.01.079>.
- Tribouillard, N., Algeo, T.J., Lyons, T., Riboulleau, A., 2006. Trace metals as paleoredox and paleoproductivity proxies: an update. *Chem. Geol.* 232, 12–32. <https://doi.org/10.1016/j.chemgeo.2006.02.012>.
- Tsang, M.Y., Böttcher, M.E., Wortmann, U.G., 2023. Estimating the effect of elemental sulfur disproportionation on the sulfur-isotope signatures in sediments. *Chem. Geol.* 632, 121533. <https://doi.org/10.1016/j.chemgeo.2022.139699>.
- Wen, H., Carignan, J., Chu, X., Fan, H., Cloquet, C., Huang, J., Zhang, Y., Chang, H., 2014. Selenium isotopes trace anoxic and ferruginous seawater conditions in the Early Cambrian. *Chem. Geol.* 390, 164–172. <https://doi.org/10.1016/j.chemgeo.2014.10.022>.
- Werne, J.P., Hollander, D.J., Behrens, A., Schaeffer, P., Albrecht, P., Sinninghe Damsté, J. S., 2000. Timing of early diagenetic sulfurization of organic matter: a precursor-product relationship in Holocene sediments of the anoxic Cariaco Basin, Venezuela. *Geochim. Cosmochim. Acta* 64, 1741–1751. [https://doi.org/10.1016/S0016-7037\(99\)00366-X](https://doi.org/10.1016/S0016-7037(99)00366-X).
- Werne, J.P., Hollander, D.J., Lyons, T.W., Sinninghe Damsté, J.S., 2004. Organic sulfur biogeochemistry: recent advances and future research directions. In: *Sulfur Biogeochemistry - Past and Present*. Geological Society of America. <https://doi.org/10.1130/0-8137-2379-5.135>.
- Werne, J.P., Lyons, T.W., Hollander, D.J., Schouten, S., Hopmans, E.C., Sinninghe Damsté, J.S., 2008. Investigating pathways of diagenetic organic matter sulfurization using compound-specific sulfur isotope analysis. *Geochim. Cosmochim. Acta* 72, 3489–3502. <https://doi.org/10.1016/j.gca.2008.04.033>.
- Wilkin, R.T., Barnes, H.L., 1996. Pyrite formation by reactions of iron monosulfides with dissolved inorganic and organic sulfur species. *Geochim. Cosmochim. Acta* 60 (21), 4167–4179. [https://doi.org/10.1016/S0016-7037\(97\)81466-4](https://doi.org/10.1016/S0016-7037(97)81466-4).
- Wing, B.A., Halevy, I., 2014. Intracellular metabolite levels shape sulfur isotope fractionation during microbial sulfate respiration. *Proc. Natl. Acad. Sci.* 111 (51), 18116–18125. <https://doi.org/10.1073/pnas.1407502111>.
- Wortmann, U.G., Bernasconi, S.M., Böttcher, M.E., 2001. Hypersulfidic deep biosphere indicates extreme sulfur isotope fractionation during single-step microbial sulfate reduction. *Geology* 29 (7), 647–650. [https://doi.org/10.1130/0091-7613\(2001\)029<0647:HDBIES>2.0.CO;2](https://doi.org/10.1130/0091-7613(2001)029<0647:HDBIES>2.0.CO;2).
- Zhabina, N.N., Volkov, I.I., 1978. A method of determination of various sulfur compounds in sea sediments and rocks. *ENV. BIOGEOCHEM. GEOMICROBIOL. 3RD INT. SYMP.: WOLFENBUETTEL; ANN ARBOR; ANN ARBOR SCI.; DA. 1978; VOL. 3, pp. 735–746.*